View metadata, citation and similar papers at core.ac.uk
brought to you by CORE
provided by DigitalCommons@CalPoly

# Description of light propagation through a circular aperture using nonparaxial vector diffraction theory

**Shekhar Guha**
*Air Force Research Laboratory, Materials and Manufacturing Directorate, Wright-Patterson Air Force Base, Dayton, Ohio, 45433, USA*
shekhar.guha@wpafb.af.mil

**Glen D. Gillen**
*Air Force Research Laboratory, Materials and Manufacturing Directorate, Anteon Corporation, Wright-Patterson Air Force Base, Dayton, Ohio, 45433, USA*
ggillen@anteon.com

**Abstract:** Using nonparaxial vector diffraction theory derived using the Hertz vector formalism, integral expressions for the electric and magnetic field components of light within and beyond an apertured plane are obtained for an incident plane wave. For linearly polarized light incident on a circular aperture, the integrals for the field components and for the Poynting vector are numerically evaluated. By further two-dimensional integration of a Poynting vector component, the total transmission of a circular aperture is determined as a function of the aperture radius to wavelength ratio. The validity of using Kirchhoff boundary conditions in the aperture plane is also examined in detail.

© 2005 Optical Society of America

**OCIS codes:** (050.1960) Diffraction theory

## References and links

1. G. R. Kirchhoff, "Zur Theorie der Lichtstrahlen," Ann. Phys. (Leipzig) **18**, 663-695 (1883).
2. A. Sommerfeld, "Zur mathematischen Theorie der Beugungsercheinungen," Nachr. Kgl. Wiss. Göttingen **4**, 338-342 (1894).
3. Lord Rayleigh, "On the passage of waves through apertures in plane screens, and allied problems," Philos. Mag. **43**, 259-272 (1897).
4. O. Mitrofanov, M. Lee, J. W. P. Hsu, L. N. Pfeifer, K. W. West, J. D. Wynn and J. F. Federici, "Terahertz pulse propagation through small apertures," App. Phys. Lett. **79**, 907–909 (2001).
5. B. Lü and K. Duan, "Nonparaxial propagation of vectorial Gaussian beams diffracted at a circular aperture," Opt. Lett **28**, 2440–2442 (2003).
6. K. Duan and B. Lü, "Vectorial nonparaxial propagation equation of elliptical Gaussian beams in the presence of a rectangular aperture," J. Opt. Sec. Am. A **21**, 1613–1620 (2004).
7. G. D. Gillen and S. Guha, "Modeling and propagation of near-field diffraction patterns: A more complete approach," Am. J. Phys. **72**, 1195–1201 (2004).
8. W. Freude and G. K. Grau, "Rayleigh-Sommerfeld and Helmholtz-Kirchhoff integrals: application to the scalar and vectorial theory of wave propagation and diffraction," J. Lightwave Technol. **13**, 24–32, (1995).
9. J. A. Stratton and L.J. Chu, "Diffraction theory of electromagnetic waves," Phys. Rev. **56**, 99–107, (1939).
10. H. A. Bethe, "Theory of diffraction by small holes," Phys. Rev. **66**, 163–182 (1944).
11. R. K. Luneberg, *Mathematical Theory of Optics* (U. California Press, Berkeley, Calif., 1964).
12. G. Bekefi, "Diffraction of electromagnetic waves by an aperture in a large screen," J. App. Phys. **24**, 1123–1130 (1953).

#6195 - $15.00 US
Received 5 January 2005; revised 18 February 2005; accepted 18 February 2005
(C) 2005 OSA

13. C. L. Andrews, "Diffraction pattern in a circular aperture measured in the microwave region," J. Appl. Phys. **21**, 761–767 (1950).
14. M. J. Ehrlich, S. Silver and G. Held,"Studies of the Diffraction of Electromagnetic waves by circular apertures and complementary obstacles: the near-zone field," J. Appl. Phys. **26**, 336–345 (1955).
15. M. Born and E. Wolf *Principles of Optics* (Cambridge University Press, Cambridge, 2003.)
16. A. Schoch, "Betrachtungen über das Schallfeld einer Kolbenmembran,"Akust. Z. **6**, 318–326 (1941).
17. A. H. Carter and A. O. Williams, Jr., "A New Expansion for the velocity potential of a piston source," J. Accoust. Soc. Am. **23**, 179–184 (1951).
18. M. Mansuripur, A. R. Zakharian and J. V. Moloney, "Interaction of light with subwavelength structures," Opt. Photonics News, 56–61 (March 2003).

## 1. Introduction

Even though the diffraction of light by an aperture is a fundamental phenomenon in optics and has been studied for a long time [1–3], it continues to be of modern interest [4–8]. It has been long recognized that 'vector' diffraction theory needs to be used to describe propagation of light in and around structures that are of the same length scale or smaller than the wavelength of light [9]. Study of diffraction of light through an aperture with a radius ($a$) comparable to the wavelength of light ($\lambda$) is a challenging phenomenon to model completely, especially for the case of $a/\lambda$ ranging between 0.1 and 10, which falls in between the theory of transmission of light through very small apertures ($a \ll \lambda$) [4, 10] and vector diffraction theory using Kirchhoff boundary conditions and high-frequency approximations [5, 6, 9, 11]. The high-frequency approximations and Kirchhoff boundary conditions assume that the light field in the aperture plane is known and is unperturbed by the presence of the aperture. While mathematically consistent and correctly predicting light distributions beyond the aperture plane, these assumptions fail to represent physical waves in the vicinity of the aperture plane and violate Maxwell's equations.

Paraxial approximations have historically been used to reduce the mathematical complexity and the computational time required for numerical integration, albeit at the cost of limiting the regions of their validity. The finite difference time domain (FDTD) method provides an accurate description of light distributions in the vicinity of the aperture without Kirchhoff or paraxial approximations, but can become computationally time-intensive at larger distances of propagation.

In this paper we show that using modern desktop computers, detailed solutions for all the electric and magnetic field components (as well as the Poynting vector) for all points in space in the aperture plane and beyond are obtainable for $a/\lambda \geq 0.1$, within a reasonable period of time (minutes) using vector diffraction theory but without invoking *any* approximations. The expressions for the field components are first obtained here as double integrals, which are valid anywhere in space within and beyond the aperture plane. Then the field components are expressed as two computationally efficient single integrals for two mutually exclusive and all-encompassing volumes of space beyond the aperture plane. Detailed two-dimensional beam profiles of the electric field and light distributions for a variety of aperture sizes and longitudinal distances are presented. The resulting three-dimensional plots provide a unique visual representation of diffraction phenomena, which had been historically hindered by the excessive computational time required. Significant differences are shown to exist between the Poynting vector components and the commonly used modulus square of the electric field. It is shown that the distribution of the electric field at and near the circular aperture is not circularly symmetric, in agreement with experimental results [12–14]. However, the field distributions obtained using the Kirchhoff boundary conditions are circularly symmetric showing that for any range of aperture to wavelength ratios, the Kirchhoff boundary conditions are invalid at and near the aperture plane. The total power transmitted through a plane parallel to the aperture plane is calculated as

#6195 - $15.00 US Received 5 January 2005; revised 18 February 2005; accepted 18 February 2005
(C) 2005 OSA

a function of the aperture size. For the specific case of points along the optical axis, analytical forms of the electromagnetic field components are derived.

## 2. Hertz vector diffraction theory (HVDT)

The electric (**E**) and magnetic (**H**) fields of an electromagnetic wave of wavelength $\lambda$ and traveling in vacuum can be determined from the polarization potential [15], or Hertz vector ($\mathbf{\Pi}$), through the relations

$$\boldsymbol{E} = k^2\mathbf{\Pi} + \boldsymbol{\nabla}(\boldsymbol{\nabla}\cdot\mathbf{\Pi}), \tag{1}$$

and

$$\mathbf{H} = -\frac{k^2}{i\omega\mu_o}\boldsymbol{\nabla}\times\mathbf{\Pi} = ik\sqrt{\frac{\varepsilon_o}{\mu_o}}\boldsymbol{\nabla}\times\mathbf{\Pi}, \tag{2}$$

where the Hertz vector is a smooth and continuous function everywhere and satisfies Maxwell's wave equation, $k = \frac{2\pi}{\lambda}$ is the wave number, and $\varepsilon_o$ and $\mu_o$ denote the vacuum permeability and permittivity constants. For the case of a plane wave which is linearly polarized (say along the $x$-direction) and propagating in the $+z$ direction, all of the **E** and **H** field components can be calculated from $\Pi_x$, the $x$-component of the Hertz vector [12], and have the following forms:

$$\begin{aligned} E_x &= k^2\Pi_x + \frac{\partial^2\Pi_x}{\partial x^2}, \\ E_y &= \frac{\partial^2\Pi_x}{\partial y\partial x}, \\ E_z &= \frac{\partial^2\Pi_x}{\partial z\partial x}, \end{aligned} \tag{3}$$

and

$$\begin{aligned} H_x &= 0, \\ H_y &= -\frac{k^2}{i\omega\mu_o}\frac{\partial\Pi_x}{\partial z} = ik\sqrt{\frac{\varepsilon_o}{\mu_o}}\frac{\partial\Pi_x}{\partial z}, \\ H_z &= \frac{k^2}{i\omega\mu_o}\frac{\partial\Pi_x}{\partial y} = -ik\sqrt{\frac{\varepsilon_o}{\mu_o}}\frac{\partial\Pi_x}{\partial y}. \end{aligned} \tag{4}$$

From the fields given in Eqs. (3) and (4) it is straight-forward to obtain the Poynting vector, **S**, where

$$\begin{aligned} \mathbf{S} &= Re\left(\mathbf{E}\times\mathbf{H}^*\right) \\ &= Re\left(E_yH_z^* - E_zH_y^*\right)\hat{i} + Re\left(-E_xH_z^*\right)\hat{j} + Re\left(E_xH_y^*\right)\hat{k}, \end{aligned} \tag{5}$$

and $\hat{i},\hat{j},\hat{k}$ denote the unit vectors in the $x$, $y$ and $z$ directions.

### 2.1. *Double integral forms for the field components*

We assume the plane wave described above is incident on an aperture which is perfectly conducting, of negligible thickness, and located in the $x$-$y$ plane at $z = 0$. Because the aperture is assumed to be conducting, it is required that the tangential components of the electric field and the normal components of the magnetic field vanish in the plane of the aperture. Applying these boundary conditions on the electromagnetic fields and requiring that the Hertz vector and the

#6195 - $15.00 US Received 5 January 2005; revised 18 February 2005; accepted 18 February 2005
(C) 2005 OSA

electromagnetic fields satisfy Maxwell's equations for all space, the Hertz vector component at the point of interest, $(x,y,z)$, is given by Bekefi [12] to be

$$\Pi_x(x,y,z) = \frac{iE_o}{2\pi k}\int\int \frac{e^{-ik\rho}}{\rho}dx_o dy_0, \tag{6}$$

where $E_o$ is the electric field amplitude of the incident plane wave and $\rho$ is the distance from a point in the aperture plane, $(x_o, y_o, 0)$, to the point of interest, or

$$\rho = \sqrt{(x-x_0)^2+(y-y_0)^2+z^2}, \tag{7}$$

and the integration is performed over the two-dimensional open aperture area.

To express the results in dimensionless parametric forms, a length scale $a$ is first chosen, and a quantity $z_0 \equiv ka^2$ and a dimensionless parameter $p_1 \equiv 2\pi a/\lambda$ are defined, along with the dimensionless coordinates $\mathbf{r_1}(x_1, y_1, z_1)$, $\mathbf{r_{01}}(x_{01}, y_{01}, 0)$, and a dimensionless variable $\rho_1$:

$$x_1 \equiv \frac{x}{a}, \quad y_1 \equiv \frac{y}{a}, \quad z_1 \equiv \frac{z}{z_0}, \quad x_{01} \equiv \frac{x_0}{a}, \quad y_{01} \equiv \frac{y_0}{a}, \tag{8}$$

$$\rho_1 \equiv \sqrt{(x_1-x_{01})^2+(y_1-y_{01})^2+p_1{}^2 z_1{}^2}. \tag{9}$$

Expressing Eq. (6) in the dimensionless form and substituting into Eqs. (3) and (4), we obtain

$$\begin{aligned}
E_x(\mathbf{r_1}) &= \frac{iE_o}{2\pi}\left[p_1 A_1(x_1,y_1,z_1) + \frac{1}{p_1}\frac{\partial^2 A_1(x_1,y_1,z_1)}{\partial x_1^2}\right], \\
E_y(\mathbf{r_1}) &= \frac{iE_o}{2\pi p_1}\frac{\partial^2 A_1(x_1,y_1,z_1)}{\partial y_1 \partial x_1}, \\
E_z(\mathbf{r_1}) &= \frac{iE_o}{2\pi p_1^2}\frac{\partial^2 A_1(x_1,y_1,z_1)}{\partial z_1 \partial x_1},
\end{aligned} \tag{10}$$

and

$$\begin{aligned}
H_x(\mathbf{r_1}) &= 0, \\
H_y(\mathbf{r_1}) &= -\frac{H_o}{2\pi p_1}\frac{\partial A_1(x_1,y_1,z_1)}{\partial z_1}, \\
H_z(\mathbf{r_1}) &= \frac{H_o}{2\pi}\frac{\partial A_1(x_1,y_1,z_1)}{\partial y_1},
\end{aligned} \tag{11}$$

where

$$A_1(\mathbf{r_1}) \equiv \int\int \frac{e^{-ip_1\rho_1}}{\rho_1}dx_{01}dy_{01} \tag{12}$$

and $H_o \equiv E_o\sqrt{\frac{\varepsilon_o}{\mu_o}}$.

Carrying out the differentiations of $A_1$ in Eqs. (10) and (11) inside the integrals in Eq. (12), the electric and magnetic field components are obtained as:

$$E_x(x_1,y_1,z_1) = \frac{iE_o p_1}{2\pi}\int\int f_1\left[(1+s_1)-(1+3s_1)\frac{(x_1-x_{01})^2}{\rho_1^2}\right]dx_{01}dy_{01}, \tag{13}$$

$$E_y(x_1,y_1,z_1) = -\frac{iE_o p_1}{2\pi}\int\int f_1(1+3s_1)\frac{(x_1-x_{01})(y_1-y_{01})}{\rho_1^2}dx_{01}dy_{01}, \tag{14}$$

$$E_z(x_1,y_1,z_1) = -\frac{iE_o p_1^2 z_1}{2\pi}\int\int f_1(1+3s_1)\frac{(x_1-x_{01})}{\rho_1^2}dx_{01}dy_{01}, \tag{15}$$

#6195 - $15.00 US Received 5 January 2005; revised 18 February 2005; accepted 18 February 2005
(C) 2005 OSA

$$H_x(x_1,y_1,z_1) = 0, \tag{16}$$

$$H_y(x_1,y_1,z_1) = -\frac{H_o p_1^3 z_1}{2\pi}\int\int f_1 s_1 dx_{01} dy_{01}, \tag{17}$$

$$H_z(x_1,y_1,z_1) = \frac{H_o p_1^2}{2\pi}\int\int f_1 s_1 (y_1 - y_{01})\, dx_{01} dy_{01}, \tag{18}$$

where

$$f_1 \equiv \frac{e^{-ip_1\rho_1}}{\rho_1} \tag{19}$$

and

$$s_1 \equiv \frac{1}{ip_1\rho_1}\left(1+\frac{1}{ip_1\rho_1}\right). \tag{20}$$

For a circular aperture of radius $a$, the limits of the integrals in Eqs. (13)–(18) are:

$$\int_{-1}^{1}\int_{-\sqrt{1-y_{01}^2}}^{\sqrt{1-y_{01}^2}} dx_{01} dy_{01}. \tag{21}$$

### *2.2. Single integral forms for the field components*

#### 2.2.1. Within the geometrically illuminated region ($r_1 < 1$)

Although the double integral forms for the electric and magnetic fields presented in the previous section give the complete solution to the Hertz vector diffraction theory for any point in space with $z_1 \geq 0$, and can be numerically evaluated in minutes on currently available desktop computers, to obtain a detailed description of the light diffracted by the aperture over a large number of points in space, it is desirable to reduce the computation time further. Schoch [16] demonstrated that the surface integral of the Hertz vector in Eq. (6) can be expressed as a line integral around the edge of the aperture for field points within the geometrically illuminated region, or $r_1 < 1$ where $r_1$ is defined below in Eq. (25). Expressing Schoch's line integral form in terms of the dimensionless parameters of Eqs. (8) and (9), the Hertz vector component for a circular aperture of radius $a$ becomes

$$\Pi_x(x_1,y_1,z_1) = \frac{E_o a^2}{p_1^2}\left[e^{-ip_1^2 z_1} - \frac{1}{2\pi}\int_0^{2\pi}\frac{e^{-ip_1 q}}{L^2}(1 - r_1\cos\phi)\, d\phi\right], \tag{22}$$

where

$$q^2(x_1,y_1,z_1,\phi) = L^2 + p_1^2 z_1^2, \tag{23}$$

$$L^2(x_1,y_1,\phi) = 1 + r_1^2 - 2r_1\cos\phi \tag{24}$$

and

$$r_1(x_1,y_1) = \sqrt{x_1^2 + y_1^2}. \tag{25}$$

Substituting Eq. (22) into Eqs. (3) and (4) the electric and magnetic field components can be expressed as

$$\begin{aligned}
E_x(x_1,y_1,z_1) &= E_o\left(e^{-ip_1^2 z_1} - \frac{1}{2\pi}\int_0^{2\pi} f_{2a}\, d\phi\right), \\
E_y(x_1,y_1,z_1) &= -\frac{E_o}{2\pi p_1^2}\int_0^{2\pi} f_{2b}\, d\phi, \\
E_z(x_1,y_1,z_1) &= -\frac{E_o}{2\pi p_1^3}\int_0^{2\pi} f_{2c}\, d\phi,
\end{aligned} \tag{26}$$

#6195 - $15.00 US Received 5 January 2005; revised 18 February 2005; accepted 18 February 2005
(C) 2005 OSA

and

$$\begin{aligned} H_x(x_1,y_1,z_1) &= 0, \\ H_y(x_1,y_1,z_1) &= H_o\left(e^{-ip_1^2 z_1} - \frac{i}{2\pi p_1^2}\int_0^{2\pi} f_{2d}\,d\phi\right), \\ H_z(x_1,y_1,z_1) &= -\frac{iH_o}{2\pi p_1}\int_0^{2\pi} f_{2e}\,d\phi, \end{aligned} \tag{27}$$

where

$$\begin{aligned} f_{2a} &\equiv \alpha\beta\gamma + \frac{1}{p_1^2}(\alpha_{11}\beta\gamma + \beta_{11}\alpha\gamma + \gamma_{11}\alpha\beta) + \frac{2}{p_1^2}(\alpha_1\beta_1\gamma + \beta_1\gamma_1\alpha + \gamma_1\alpha_1\beta), \\ f_{2b} &\equiv \alpha_{12}\beta\gamma + \beta_{12}\alpha\gamma + \gamma_{12}\alpha\beta \\ &\quad + \alpha(\beta_1\gamma_2 + \gamma_1\beta_2) + \beta(\alpha_1\gamma_2 + \gamma_1\alpha_2) + \gamma(\alpha_1\beta_2 + \beta_1\alpha_2), \\ f_{2c} &\equiv \alpha_{13}\beta\gamma + \alpha_3(\beta\gamma_1 + \gamma\beta_1), \\ f_{2d} &\equiv \alpha_3\beta\gamma, \\ f_{2e} &\equiv \alpha_2\beta\gamma + \beta_2\alpha\gamma + \gamma_2\alpha\beta. \end{aligned} \tag{28}$$

The variables $\alpha$, $\beta$ and $\gamma$ are defined as

$$\begin{aligned} \alpha &\equiv e^{-ip_1 q}, \\ \beta &\equiv \frac{1}{L^2}, \\ \gamma &\equiv 1 - r_1\cos\phi. \end{aligned} \tag{29}$$

The subscripts of $\alpha$, $\beta$ and $\gamma$ in Eq. (28) correspond to partial derivatives; for example,

$$\begin{aligned} \alpha_1 = \frac{\partial\alpha}{\partial x_1}, \quad \alpha_2 = \frac{\partial\alpha}{\partial y_1}, \quad \alpha_3 = \frac{\partial\alpha}{\partial z_1}, \\ \alpha_{11} = \frac{\partial^2\alpha}{\partial x_1^2}, \quad \alpha_{12} = \frac{\partial^2\alpha}{\partial y_1\partial x_1}, \text{ etc.} \end{aligned} \tag{30}$$

The partial derivative terms of $\alpha$ are

$$\alpha_1 \equiv -ip_1\alpha q_1, \quad \alpha_2 \equiv -ip_1\alpha q_2, \quad \alpha_3 \equiv -ip_1\alpha q_3, \tag{31}$$

$$\alpha_{11} \equiv -ip_1(\alpha_1 q_1 + \alpha q_{11}),\ \alpha_{12} \equiv -ip_1(\alpha_2 q_1 + \alpha q_{12}),\ \alpha_{13} \equiv -ip_1(\alpha_3 q_1 + \alpha q_{13}), \tag{32}$$

where

$$q_1 \equiv \frac{x_1\delta}{q}, \quad q_2 \equiv \frac{y_1\delta}{q}, \quad q_3 \equiv \frac{p_1^2 z_1}{q}, \tag{33}$$

$$q_{11} \equiv \frac{\delta}{q} + \frac{x_1^2}{q}\left(\frac{\cos\phi}{r_1^3} - \frac{\delta^2}{q^2}\right), \tag{34}$$

$$q_{12} \equiv \frac{x_1 y_1}{q}\left(\frac{\cos\phi}{r_1^3} - \frac{\delta^2}{q^2}\right), \quad q_{13} \equiv -p_1^2 x_1 z_1\frac{\delta}{q^3} \tag{35}$$

#6195 - $15.00 US Received 5 January 2005; revised 18 February 2005; accepted 18 February 2005
(C) 2005 OSA

and

$$\delta \equiv \frac{r_1 - \cos\phi}{r_1}. \tag{36}$$

The partial derivative terms of $\beta$ are

$$\beta_1 \equiv -\frac{2L_1}{L^3}, \quad \beta_2 \equiv -\frac{2L_2}{L^3}, \tag{37}$$

$$\beta_{11} \equiv \frac{6L_1^2}{L^4} - \frac{2L_{11}}{L^3}, \quad \beta_{12} \equiv \frac{6L_1L_2}{L^4} - \frac{2L_{12}}{L^3}, \tag{38}$$

where

$$L_1 \equiv \frac{x_1\delta}{L}, \quad L_2 \equiv \frac{y_1\delta}{L}, \tag{39}$$

$$L_{11} \equiv \frac{\delta}{L} + \frac{x_1^2}{L}\left(\frac{\cos\phi}{r_1^3} - \frac{\delta^2}{L^2}\right), \quad L_{12} \equiv \frac{x_1y_1}{L}\left(\frac{\cos\phi}{r_1^3} - \frac{\delta^2}{L^2}\right). \tag{40}$$

The partial derivative terms of $\gamma$ are

$$\gamma_1 \equiv -\frac{x_1\cos\phi}{r_1}, \quad \gamma_2 \equiv -\frac{y_1\cos\phi}{r_1}, \tag{41}$$

$$\gamma_{11} \equiv -\frac{\cos\phi}{r_1}\left(1 - \frac{x_1^2}{r_1^2}\right), \quad \gamma_{12} \equiv \frac{x_1y_1\cos\phi}{r_1^3}. \tag{42}$$

2.2.2. Within the geometrical shadow region ($r_1 > 1$)

For points of interest in the geometrical shadow region, or where $z_1 \geq 0$ and $r_1 > 1$, Carter and Williams [17] demonstrated that the double integral of the Hertz vector component in Eq. (6) can also be expressed as a single integral. Using the Carter and Williams' integral form (Eq. 12 of Ref. [17]) for the double integral in Eq. (6), the Hertz vector component can be expressed as

$$\Pi_x(x_1,y_1,z_1) = \frac{a^2E_o}{\pi p_1^2}\int_0^{\pi/2}\frac{u}{v}\cos\psi d\psi, \tag{43}$$

where

$$u \equiv e^{-ip_1g} - e^{-ip_1h}, \quad v \equiv \sqrt{r_1^2 - \sin^2\psi}, \tag{44}$$

and

$$g \equiv \sqrt{p_1^2z_1^2 + (v + \cos\psi)^2}, \quad h \equiv \sqrt{p_1^2z_1^2 + (v - \cos\psi)^2}. \tag{45}$$

Substituting Eq. (43) into Eqs. (3) and (4) the electric and magnetic field components become

$$\begin{aligned} E_x(x_1,y_1,z_1) &= \frac{E_o}{\pi}\int_0^{\pi/2} f_{3a}d\psi, \\ E_y(x_1,y_1,z_1) &= \frac{E_o}{\pi p_1^2}\int_0^{\pi/2} f_{3b}d\psi, \\ E_z(x_1,y_1,z_1) &= \frac{E_o}{\pi p_1^3}\int_0^{\pi/2} f_{3c}d\psi, \end{aligned} \tag{46}$$

#6195 - $15.00 US Received 5 January 2005; revised 18 February 2005; accepted 18 February 2005
(C) 2005 OSA

and

$$\begin{aligned} H_x(x_1,y_1,z_1) &= 0, \\ H_y(x_1,y_1,z_1) &= \frac{iH_o}{\pi p_1^2}\int_0^{\pi/2} f_{3d}\,d\psi, \\ H_z(x_1,y_1,z_1) &= -\frac{iH_o}{\pi p_1}\int_0^{\pi/2} f_{3e}\,d\psi, \end{aligned} \tag{47}$$

where

$$\begin{aligned} f_{3a} &\equiv \frac{\cos\psi}{v}\left[u+\frac{1}{p_1^2}\left(u_{11}-\frac{2x_1u_1}{v^2}+\frac{3ux_1^2}{v^4}-\frac{u}{v^2}\right)\right], \\ f_{3b} &\equiv \frac{\cos\psi}{v}\left(u_{12}-\frac{y_1u_1}{v^2}+\frac{3x_1y_1u}{v^4}-\frac{x_1u_2}{v^2}\right), \\ f_{3c} &\equiv \frac{\cos\psi}{v}\left(u_{13}-\frac{x_1u_3}{v^2}\right), \\ f_{3d} &\equiv \frac{\cos\psi}{v}u_3, \\ f_{3e} &\equiv \frac{\cos\psi}{v}\left(u_2-\frac{y_1u}{v^2}\right). \end{aligned} \tag{48}$$

The subscripts of $u$ correspond to partial derivatives (as in Eq. (30)):

$$u_1 \equiv -ip_1\left(g_1e^{-ip_1g}-h_1e^{-ip_1h}\right), \quad u_2 \equiv -ip_1\left(g_2e^{-ip_1g}-h_2e^{-ip_1h}\right), \tag{49}$$

$$u_3 \equiv -ip_1^3z_1\left(\frac{e^{-ip_1g}}{g}-\frac{e^{-ip_1h}}{h}\right), \tag{50}$$

$$\begin{aligned} u_{11} &\equiv -ip_1\left(g_{11}e^{-ip_1g}-h_{11}e^{-ip_1h}\right)-p_1^2\left(g_1^2e^{-ip_1g}-h_1^2e^{-ip_1h}\right), \\ u_{12} &\equiv -ip_1\left(g_{12}e^{-ip_1g}-h_{12}e^{-ip_1h}\right)-p_1^2\left(g_1g_2e^{-ip_1g}-h_1h_2e^{-ip_1h}\right), \\ u_{13} &\equiv -ip_1\left(g_{13}e^{-ip_1g}-h_{13}e^{-ip_1h}\right)-p_1^2\left(g_1g_3e^{-ip_1g}-h_1h_3e^{-ip_1h}\right), \end{aligned} \tag{51}$$

where

$$g_1 \equiv x_1g_a, \quad g_2 \equiv y_1g_a, \quad g_3 \equiv \frac{z_1p_1^2}{g}, \tag{52}$$

$$g_{11} \equiv g_a-\frac{x_1^2}{g}\left(g_a^2+\frac{\cos\psi}{v^3}\right), \; g_{12} \equiv -\frac{x_1y_1}{g}\left(g_a^2+\frac{\cos\psi}{v^3}\right), \; g_{13} \equiv -\frac{x_1z_1p_1^2}{g^2}g_a, \tag{53}$$

$$h_1 \equiv x_1h_a, \quad h_2 \equiv y_1h_a, \quad h_3 \equiv \frac{z_1p_1^2}{h}, \tag{54}$$

$$h_{11} \equiv h_a-\frac{x_1^2}{h}\left(h_a^2-\frac{\cos\psi}{v^3}\right), \; h_{12} \equiv -\frac{x_1y_1}{h}\left(h_a^2-\frac{\cos\psi}{v^3}\right), \; h_{13} \equiv -\frac{x_1z_1p_1^2h_a}{g^2}, \tag{55}$$

and

$$g_a \equiv \frac{v+\cos\psi}{vg}, \quad h_a \equiv \frac{v-\cos\psi}{vh}. \tag{56}$$

Even though the single integral expressions for **E** and **H** (Eqs. (26), (27), (46) and (47)) involve a large number of terms, they can be evaluated significantly (10 to 15 times) faster than the double integral expressions (Eqs. (13)–(18)).

#6195 - $15.00 US Received 5 January 2005; revised 18 February 2005; accepted 18 February 2005
(C) 2005 OSA

## 3. Vector diffraction theory using Kirchhoff boundary conditions (KVDT)

The Hertz vector diffraction theory (HVDT) described above provides the values of the electromagnetic fields in the aperture plane and beyond. The Kirchhoff boundary conditions, on the other hand, *specify* the values of the fields in the aperture plane. Starting from these specified values at $z = 0$ the fields for $z > 0$ can be obtained using the Green's function method of solution of the wave equation. Luneberg [11] has shown how the Green's function method can be used to derive the longitudinal component ($E_z$) of the fields from the known transverse components in the aperture plane.

Luneberg's method has recently been used by Lü and Duan [5, 6] to derive analytical expressions for the electric field components of diffracted waves beyond the aperture. However, despite the claim in Refs. [5, 6] that the treatment of the problem is nonparaxial, the analytical expressions derived there are based upon the assumption that the on-axis distance to the point of interest is large compared to the radial distance (Eq. 6 in Lü and Duan [5] and Eq. 7 in Duan and Lü [6]). Here we derive the vector components of the electric and magnetic fields in terms of double integrals in dimensionless parameters for incident planar beam distributions of arbitrary shape, using the Kirchhoff boundary conditions, with the aim of determining the region of their validity. Neither the paraxial (Fresnel) approximation nor the approximations used by Lü and Duan [5, 6] are invoked here.

Given a beam of light whose electric field distribution in the plane $z = 0$ is known in terms of the coordinates $x_0$ and $y_0$ in the plane as $\mathbf{E} = E_x(\mathbf{r_0})\hat{i} + E_y(\mathbf{r_0})\hat{j}$, the field at a point $\mathbf{r} = x\hat{i} + y\hat{j} + z\hat{k}$ is given by [11]

$$E_x(\mathbf{r}) = -\frac{1}{2\pi}\int\int_{-\infty}^{\infty} E_x(\mathbf{r_0})\frac{\partial G(\mathbf{r},\mathbf{r_0})}{\partial z}dx_0dy_0, \tag{57}$$

$$E_y(\mathbf{r}) = -\frac{1}{2\pi}\int\int_{-\infty}^{\infty} E_y(\mathbf{r_0})\frac{\partial G(\mathbf{r},\mathbf{r_0})}{\partial z}dx_0dy_0, \tag{58}$$

where $\mathbf{r_0} = x_0\hat{i} + y_0\hat{j}$. The Green's function $G$ used in Eqs. (57) and (58) is given by

$$G(\mathbf{r},\mathbf{r_0}) = \frac{e^{-ik\rho}}{\rho}, \tag{59}$$

and the distance $\rho$ is defined in Eq. (7).

Using Eqs. (57) and (58) in the Maxwell equation $\nabla\cdot\mathbf{E} = 0$ in charge-free space, i.e.,

$$\frac{\partial E_z}{\partial z} = -\left(\frac{\partial E_x}{\partial x} + \frac{\partial E_y}{\partial y}\right), \tag{60}$$

and interchanging the orders of the partial derivatives of G, we obtain

$$\begin{aligned} 2\pi\frac{\partial E_z}{\partial z} &= \int\int_{-\infty}^{\infty}\left(E_x(\mathbf{r_0})\frac{\partial^2 G}{\partial x\partial z} + E_y(\mathbf{r_0})\frac{\partial^2 G}{\partial y\partial z}\right)dx_0dy_0 \\ &= \frac{\partial}{\partial z}\left[\int\int_{-\infty}^{\infty}\left(E_x(\mathbf{r_0})\frac{\partial G}{\partial x} + E_y(\mathbf{r_0})\frac{\partial G}{\partial y}\right)dx_0dy_0\right]. \end{aligned} \tag{61}$$

From Eq. (61), $E_z$ is obtained as

$$E_z(\mathbf{r}) = \frac{1}{2\pi}\int\int_{-\infty}^{\infty}\left(E_x(\mathbf{r_0})\frac{\partial G}{\partial x} + E_y(\mathbf{r_0})\frac{\partial G}{\partial y}\right)dx_0dy_0 + F_1(x,y), \tag{62}$$

where $F_1(x,y)$ is a function to be determined from the boundary conditions. The term $F_1(x,y)$, was ignored in previous treatments [5, 6, 11], and is necessary for $E_z$ to approach the imposed boundary condition as $z$ approaches 0.

#6195 - $15.00 US Received 5 January 2005; revised 18 February 2005; accepted 18 February 2005
(C) 2005 OSA

Using the length scale $a$, the quantity $z_0 \equiv ka^2$, the dimensionless parameter $p_1 \equiv 2\pi a/\lambda$, and the normalized units of Eqs. (8) and (9) as before, and the expression for the Green's function from Eq. (59), the three components of the electric field vector can now be rewritten as

$$\begin{aligned}
E_x(\mathbf{r_1}) &= -\frac{p_1^3 z_1}{2\pi}\int\int_{-\infty}^{\infty} E_x(\mathbf{r_{01}}) f_1 s_1 dx_{01} dy_{01}, \\
E_y(\mathbf{r_1}) &= -\frac{p_1^3 z_1}{2\pi}\int\int_{-\infty}^{\infty} E_y(\mathbf{r_{01}}) f_1 s_1 dx_{01} dy_{01}, \\
E_z(\mathbf{r_1}) &= \frac{p_1^2}{2\pi}\Big[\int\int_{-\infty}^{\infty}\Big( E_x(\mathbf{r_{01}})(x_1 - x_{01}) \\
&\quad + E_y(\mathbf{r_{01}})(y_1 - y_{01})\Big) f_1 s_1 dx_{01} dy_{01}\Big] + F_1(x_1, y_1),
\end{aligned} \tag{63}$$

where $f_1$ and $s_1$ are defined in Eqs. (19) and (20).

The magnetic field components can be derived similarly to the derivation of the electric field components using Green's theorem in Eqs. (57) - (62), yielding

$$\begin{aligned}
H_x(\mathbf{r_1}) &= -\frac{p_1^3 z_1}{2\pi}\int\int_{-\infty}^{\infty} H_x(\mathbf{r_{01}}) f_1 s_1 dx_{01} dy_{01}, \\
H_y(\mathbf{r_1}) &= -\frac{p_1^3 z_1}{2\pi}\int\int_{-\infty}^{\infty} H_y(\mathbf{r_{01}}) f_1 s_1 dx_{01} dy_{01}, \\
H_z(\mathbf{r_1}) &= \frac{p_1^2}{2\pi}\Big[\int\int_{-\infty}^{\infty}\Big( H_x(\mathbf{r_{01}})(x_1 - x_{01}) \\
&\quad + H_y(\mathbf{r_{01}})(y_1 - y_{01})\Big) f_1 s_1 dx_{01} dy_{01}\Big] + F_2(x_1, y_1),
\end{aligned} \tag{64}$$

where $F_2(x_1, y_1)$ is a function to be determined from the boundary conditions. Using Eqs. (63) and (64) the Poynting vector components can be calculated from Eq. (5).

In the Kirchhoff formalism [9] the field components on the dark side of the screen are assumed to be zero except at the opening, where they have their undisturbed values that they would have had in the absence of the screen. For a linearly polarized plane wave light beam (say with **E** in the $x$-direction, and **H** in the $y$-direction) incident on a circular aperture of radius $a$ in an opaque screen, the electric field components just at the exit of the aperture (at the $z = 0$ plane) are then

$$\begin{aligned}
E_x(x_{01}, y_{01}, 0) &= \begin{cases} E_0 & \text{if } x_{01}^2 + y_{01}^2 < 1 \\ 0 & \text{otherwise} \end{cases} \\
E_y(x_{01}, y_{01}, 0) &= 0 \\
E_z(x_{01}, y_{01}, 0) &= 0,
\end{aligned} \tag{65}$$

and the magnetic field components are

$$\begin{aligned}
H_x(x_{01}, y_{01}, 0) &= 0 \\
H_y(x_{01}, y_{01}, 0) &= \begin{cases} H_0 & \text{if } x_{01}^2 + y_{01}^2 < 1 \\ 0 & \text{otherwise} \end{cases} \\
H_z(x_{01}, y_{01}, 0) &= 0.
\end{aligned} \tag{66}$$

Inserting Eqs. (65) and (66) in Eqs. (63) and (64), the expressions for the electric and magnetic fields are obtained:

$$E_x(x_1, y_1, z_1) = -E_0 \frac{p_1^3 z_1}{2\pi} B_1(x_1, y_1, z_1), \tag{67}$$

#6195 - $15.00 US Received 5 January 2005; revised 18 February 2005; accepted 18 February 2005
(C) 2005 OSA

$$E_y(x_1,y_1,z_1) = 0, \tag{68}$$

$$E_z(x_1,y_1,z_1) = E_0\frac{p_1^2}{2\pi}\left[B_2(x_1,y_1,z_1)-B_2(x_1,y_1,0)\right], \tag{69}$$

and

$$H_x(x_1,y_1,z_1) = 0, \tag{70}$$

$$H_y(x_1,y_1,z_1) = -H_0\frac{p_1^3 z_1}{2\pi}B_1(x_1,y_1,z_1), \tag{71}$$

$$H_z(x_1,y_1,z_1) = H_0\frac{p_1^2}{2\pi}\left[B_3(x_1,y_1,z_1)-B_3(x_1,y_1,0)\right], \tag{72}$$

where

$$B_1(x_1,y_1,z_1) = \int_{-1}^{1}\int_{-\sqrt{1-y_{01}^2}}^{\sqrt{1-y_{01}^2}} f_1 s_1 dx_{01}dy_{01}, \tag{73}$$

$$B_2(x_1,y_1,z_1) = \int_{-1}^{1}\int_{-\sqrt{1-y_{01}^2}}^{\sqrt{1-y_{01}^2}} f_1 s_1 (x_1-x_{01})dx_{01}dy_{01}, \tag{74}$$

$$B_3(x_1,y_1,z_1) = \int_{-1}^{1}\int_{-\sqrt{1-y_{01}^2}}^{\sqrt{1-y_{01}^2}} f_1 s_1 (y_1-y_{01})dx_{01}dy_{01}. \tag{75}$$

The terms $B_2(x_1,y_1,0)$ and $B_3(x_1,y_1,0)$ in Eqs. (69) and (72) arise from the presence of the terms $F_1(x_1,y_1)$ and $F_2(x_1,y_1)$ in Eqs. (62)–(64). They ensure that the boundary conditions $E_z = H_z = 0$ at $z_1 = 0$ (Eqs. (65) and (66)) are valid. As mentioned earlier, they have been ignored in Refs.[5, 6, 11], so that the calculated longitudinal field components $E_z$ and $H_z$ obtained there do not vanish at $z_1 = 0$, contradicting the boundary condition.

It should be noted that both the $E_x$ and $H_y$ KVDT integrals (Eqs. (67), (71) and (73)) have the same form as the $H_y$ HVDT double integral (Eq. (17)) and one of the four integral terms of the HVDT $E_x$ component (Eq. (13)), and are radially symmetric with respect to $x_1$ and $y_1$. Therefore the calculated fields of $E_x$ and $H_y$ using KVDT will always have radial symmetry and are independent of the orientation of the polarization for normally incident light. In contrast, the HVDT method shows (Eqs. (13)–(18)) that the components of all the electromagnetic fields except $H_x$ and $H_y$ are dependent on the direction of the incident polarization.

## 4. Analytical on-axis expressions and calculations

### *4.1. Analytical on-axis expressions using HVDT*

Starting with the Hertz vector diffraction theory, analytical expressions for the components of **E** and **H** for on-axis positions and $z_1 \geq 0$ can be obtained by direct integration. Using Eqs. (3) and (6) the on-axis integral expression for $E_x$ can be found to be

$$E_x(0,0,z_1) = E_o\frac{i}{2\pi}\left[\int\int\left(p_1\frac{e^{-ip_1r_2}}{r_2}-i\frac{e^{-ip_1r_2}}{r_2^2}-\frac{e^{-ip_1r_2}}{p_1r_2^3}-p_1x_{01}^2\frac{e^{-ip_1r_2}}{r_2^2}\right.\right.$$
$$\left.\left.+3ix_{01}^2\frac{e^{-ip_1r_2}}{r_2^4}+3x_{01}^2\frac{e^{-ip_1r_2}}{p_1r_2^5}\right)dx_{01}dy_{01}\right], \tag{76}$$

where

$$r_2 = \sqrt{x_{01}^2+y_{01}^2+p_1^2z_1^2}. \tag{77}$$

#6195 - $15.00 US Received 5 January 2005; revised 18 February 2005; accepted 18 February 2005
(C) 2005 OSA

After converting to polar coordinates and integrating the angular terms, the radial integral is integrated by parts where the definite integral from each term in Eq. (76) cancels with that of another term's definite integral. The resulting analytical expression for the on-axis $x$-component of the electric field becomes

$$\begin{aligned} E_x(0,0,z_1) &= E_o \frac{i}{2}\left[ i(e_1-e_2) - \frac{1}{p_1}\left(\frac{e_1}{d_1}-\frac{e_2}{d_2}\right)\right. \\ &\left. + ip_1^2 z_1^2\left(\frac{e_1}{d_1^2}-\frac{e_2}{d_2^2}\right) + p_1 z_1^2\left(\frac{e_1}{d_1^3}-\frac{e_2}{d_2^3}\right)\right], \end{aligned} \tag{78}$$

where

$$\begin{aligned} e_1 &= e^{-ip_1\sqrt{1+p_1^2 z_1^2}}, \\ e_2 &= e^{-ip_1^2 z_1}, \\ d_1 &= \sqrt{1+p_1^2 z_1^2}, \\ d_2 &= p_1 z_1. \end{aligned} \tag{79}$$

Similarly, for on-axis points the double integral expression for the $y$-component of the magnetic field becomes

$$H_y(0,0,z_1) = H_o \frac{p_1 z_1}{2\pi}\int\int\left(ip_1\frac{e^{-ip_1 r_2}}{r_2^2}+\frac{e^{-ip_1 r_2}}{r_2^3}\right)dx_{01}dy_{01}, \tag{80}$$

which can be integrated to

$$H_y(0,0,z_1) = H_o\left(e^{-ip_1^2 z_1} - p_1 z_1\frac{e^{-ip_1\sqrt{1+p_1^2 z_1^2}}}{\sqrt{1+p_1^2 z_1^2}}\right). \tag{81}$$

Using Eqs. (78) and (81) the $z$-component of the Poynting vector can be evaluated for on-axis points.

At the center of the circular aperture the real and imaginary components of $E_x$ reduce to

$$\text{Real}\left[E_x(0,0,0)\right] = E_o\left[1-\frac{1}{2}\left(\cos p_1 + \frac{\sin p_1}{p_1}\right)\right] \tag{82}$$

and

$$\text{Imaginary}\left[E_x(0,0,0)\right] = -\frac{E_o}{2}\left(\frac{\cos p_1}{p_1} - \sin p_1\right), \tag{83}$$

while $H_y/H_o$ approaches unity for all values of $p_1$.

### *4.2. Analytical on-axis expressions using KVDT*

For on-axis points ($x_1 = y_1 = 0$) the non-zero components of the fields evaluated from the KVDT integral term $B_1$ (Eq. (73)) also reduce to the analytical forms:

$$E_x(0,0,z_1) = E_o\left(e^{-ip_1^2 z_1} - p_1 z_1\frac{e^{-ip_1\sqrt{1+p_1^2 z_1^2}}}{\sqrt{1+p_1^2 z_1^2}}\right), \tag{84}$$

and

$$H_y(0,0,z_1) = H_o\left(e^{-ip_1^2 z_1} - p_1 z_1\frac{e^{-ip_1\sqrt{1+p_1^2 z_1^2}}}{\sqrt{1+p_1^2 z_1^2}}\right). \tag{85}$$

#6195 - $15.00 US Received 5 January 2005; revised 18 February 2005; accepted 18 February 2005
(C) 2005 OSA

As $z_1$ approaches the aperture plane, both $E_x/E_o$ and $H_y/H_o$ approach unity and are independent of the value of $p_1$ and the orientation of the incident polarization.

The KVDT integrals $B_2$ and $B_3$ are identically equal to zero for $x_1 = y_1 = 0$, so that the longitudinal components $E_z$ and $H_z$ vanish for on-axis points, and the Poynting vector only has a $z$-component, or

$$\mathbf{S}(0,0,z_1) = S_0 \left( \frac{1+2p_1^2 z_1^2}{1+p_1^2 z_1^2} - \frac{2p_1 z_1}{\sqrt{1+p_1^2 z_1^2}} \cos\left[ p_1^2 z_1 \left( \sqrt{1+\frac{1}{p_1^2 z_1^2}} - 1 \right) \right] \right) \hat{k}, \tag{86}$$

where

$$S_o \equiv E_o H_o^* = \sqrt{\frac{\varepsilon_o}{\mu_o}} |E_o|^2 \tag{87}$$

denotes the intensity of the incident undisturbed beam.

Due to the cosine term in Eq. (86), the on-axis value of the Poynting vector oscillates with $z_1$ for $p_1 > \pi$, with locations of the maxima and the minima given by

$$z_{1m} = \frac{p_1^2 - m^2\pi^2}{2m\pi p_1^2}, \tag{88}$$

where $m$ has integer values from 1 to $p_1/\pi$. Odd values of $m$ correspond to maxima and even values correspond to minima. The value of $m = 1$ gives the location of the on-axis maximum farthest from the aperture, and is roughly $1/(2\pi)$ for large values of $p_1$.

## 5. Power transmission function

The radiative power transmitted through a surface normal to the $z$-axis is given by

$$P_z(z_1) \quad = \quad \int_{-\infty}^{\infty} \int_{-\infty}^{\infty} S_z(x_1, y_1, z_1)\, dx_1 dy_1. \tag{89}$$

Defining $P_o \equiv \pi a^2 S_o$ as the amount of unperturbed incident power that would be intercepted by the aperture, the power transmission function of the aperture, $T$, is given by

$$T \equiv \frac{P_z}{P_o} \quad = \quad \frac{1}{P_o} \int_{-\infty}^{\infty} \int_{-\infty}^{\infty} S_z(x_1, y_1, z_1)\, dx_1 dy_1, \tag{90}$$

where $S_z$ is determined from the calculated values of $\mathbf{E}$ and $\mathbf{H}$ for a given value of $a/\lambda$.

## 6. Calculation of electromagnetic fields and Poynting vectors

In this section the results of the calculations of the electromagnetic field integrals are presented. The expressions derived in sections 2–5 were calculated on commonly available desktop computers (2.4 GHz Pentium processor) using the commercial software Mathcad. The tolerance of integration in Mathcad was typically set between $10^{-3}$ and $10^{-5}$. The calculation time required to run the single integral expressions was found to be approximately 10 to 15 times faster than that required for a calculation using the double integral expressions.

### *6.1. Beam distributions in the aperture plane*

Figures 1–9 show the distributions of the normalized fields and normalized axial Poynting vector component, $S_z/S_o$, in the aperture plane. These results were obtained from the previously derived integral expressions by setting $z_1 = 10^{-5}$ and making sure that the values of the integrals

#6195 - $15.00 US Received 5 January 2005; revised 18 February 2005; accepted 18 February 2005
(C) 2005 OSA

were unchanged when a smaller value of $z_1$ was chosen. A convention adopted in the following figures is that in each graph, solid lines denote the real components and the dotted lines denote the imaginary components of the fields.

Figure 1 shows the calculation of the $x$-component of the electric field in the aperture plane as a function of $x_1$ and $y_1$, for $a/\lambda = 5$. The calculated $E_x$ field is seen to exhibit radial asymmetry in agreement with experimental measurements by Andrews [13] and Ehrlich *et al.* [14] in the aperture plane for diffraction of microwave radiation. The number of oscillations of $E_x$ along the $y$-axis from the center of the aperture to the edge is equal to the aperture to wavelength ratio, $a/\lambda$. Along with the strong asymmetry in the $x$ and $y$-directions, it is seen that the value of the real part of $E_x$ at the center of the aperture is $E_o/2$, whereas according to Kirchhoff approximations, $E_x$ should be equal to $E_o$ everywhere in the aperture. The real and imaginary parts of $E_x(0,0,0)$ obtained from Eqs. (82) and (83), are plotted as a function of $a/\lambda$ in Figs. 2(a) and (b), respectively. Figure 2 shows that at the aperture plane, the Kirchhoff approximation is not valid even for large values of $a/\lambda$, with the real part of $E_x$ oscillating between 0.5 and 1.5, for all $a/\lambda > 0.5$. The oscillations of Fig. 2, which continue indefinitely as $p_1$ increases, with values of 1.5 occurring for $a/\lambda$ values having half-integer values, and 0.5 for integer values, have previously been experimentally demonstrated [14]. Eq. (83) also shows that as $p_1$, i.e. $a/\lambda$, goes to zero, the value of the imaginary part of $E_x(0,0,0)$ diverges as $1/p_1$, thereby implying that the HVDT theory described here is invalid for small $p_1$ ($< 0.1$.) The results presented here match the experimental measurements for $a/\lambda \geq 0.5$ shown in Ref. [12–14]. The present HVDT results may therefore be considered to be valid for $a/\lambda \geq 0.5$.

Figure 1 also shows that near the rim of the aperture the imaginary component of $E_x$ increases rapidly in magnitude, causing the modulus square of the electric field to diverge as $x_1 \rightarrow \pm 1$. At the same positions in space however, $H_y$ rapidly approaches zero. The resulting $z$-component of the Poynting vector, $S_z$, has a smooth and continuous transition across the rim of the aperture, unlike $|E_x|^2$, as illustrated in Fig. 3(a). There are also significant differences between $|E_x|^2$ and $S_z$ in the aperture plane along the $y$-axis, as shown in Fig. 3(b). The values of $E_x$ and $H_y$ displayed in Fig. 3 were calculated using Eqs. (26) and (27) for $r_1 < 1$ and Eqs. (46) and (47) for $r_1 > 1$. Other electromagnetic field components ($E_y$, $E_z$ and $H_z$) also possess some structure in the aperture plane, but with negligible ($< 10^{-3}$) magnitudes.

The expression of the Hertz vector integrals in the single integral forms allow detailed calculations of the light intensity distribution in the aperture plane (as well as beyond it) as shown in Figs. 4–9. To obtain adequate resolution in these two-dimensional plots, 200 by 200 single integrals were calculated for each quadrant which took approximately four hours to run. Calculation of the intensity values over an array of the same size using the double integrals took approximately 60 hours.

To emphasize the difference between the squared modulus of the electric field, $|E_x|^2$, and the Poynting vector component, $S_z$, the two-dimensional distribution of $|E_x/E_o|^2$ and $S_z/S_o$ are plotted in Figs. 4 and 5, respectively, both for $a/\lambda = 5$. As mentioned before, even in the aperture plane, the transition of the Poynting vector component $S_z$ between the illuminated and the dark region is smooth, whereas according to the Kirchhoff boundary conditions, there is a sharp discontinuity of the electric field (as well as $S_z$) at the boundary.

In Figs. 6–9, the $x$-$y$ distribution of $S_z$ in the aperture plane is plotted for $a/\lambda = 2.5$, 2, 1, and 0.5, respectively. From the center of the aperture out to the rim along the $y$-axis, the number of oscillations of $S_z$ equals the value of $a/\lambda$. Figure 9 illustrates that for $a/\lambda < 1$ the oscillatory behavior of $E_x$, and subsequently $S_z$, in the aperture plane have been eliminated, and an ellipticity in the beam profile has become the dominant characteristic.

#6195 - $15.00 US Received 5 January 2005; revised 18 February 2005; accepted 18 February 2005
(C) 2005 OSA

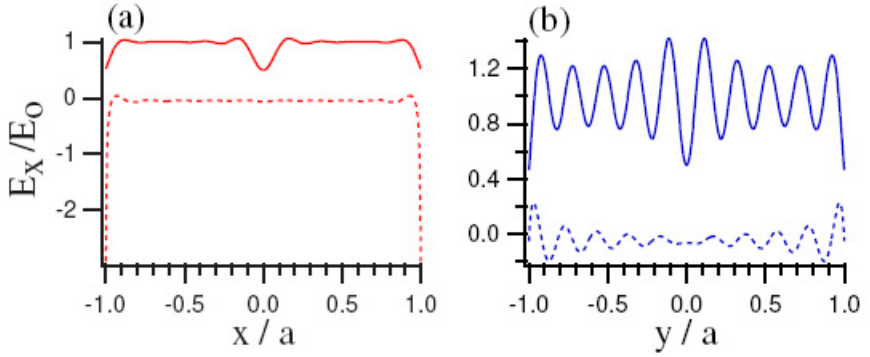


Fig. 1. The real (solid lines) and the imaginary (dashed lines) $x$-components of the normalized electric field versus (a) the $x$-position and (b) the $y$-position in the aperture plane, calculated using the single integral HVDT for $a/\lambda = 5$.

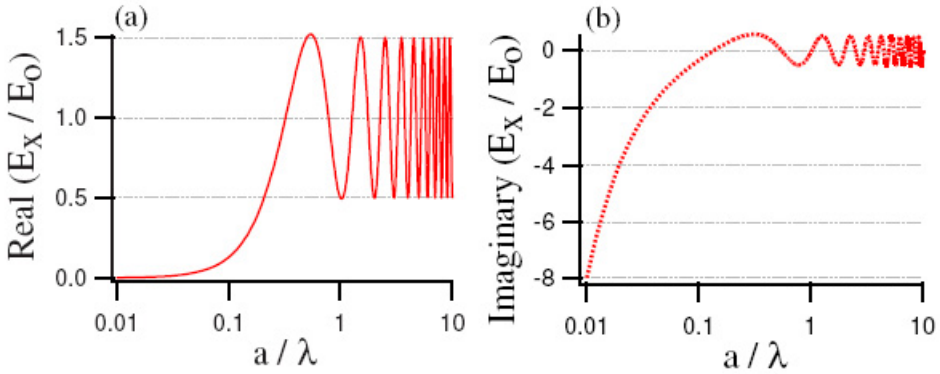


Fig. 2. The real component, part (a), and the imaginary component, part (b), of the normalized electric field at the center of the aperture plane, (0,0,0), versus the aperture to wavelength ratio, $a/\lambda$.

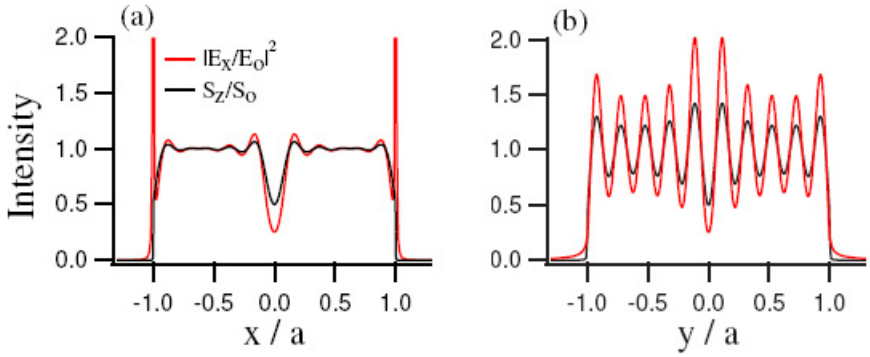


Fig. 3. The modulus square of the $x$-component of the electric field (red lines) and the $z$-component of the Poynting vector (black lines) versus (a) the $x$-position and (b) the $y$-position in the aperture plane, calculated using the single integral HVDT for $a/\lambda = 5$.

#6195 - $15.00 US Received 5 January 2005; revised 18 February 2005; accepted 18 February 2005
(C) 2005 OSA

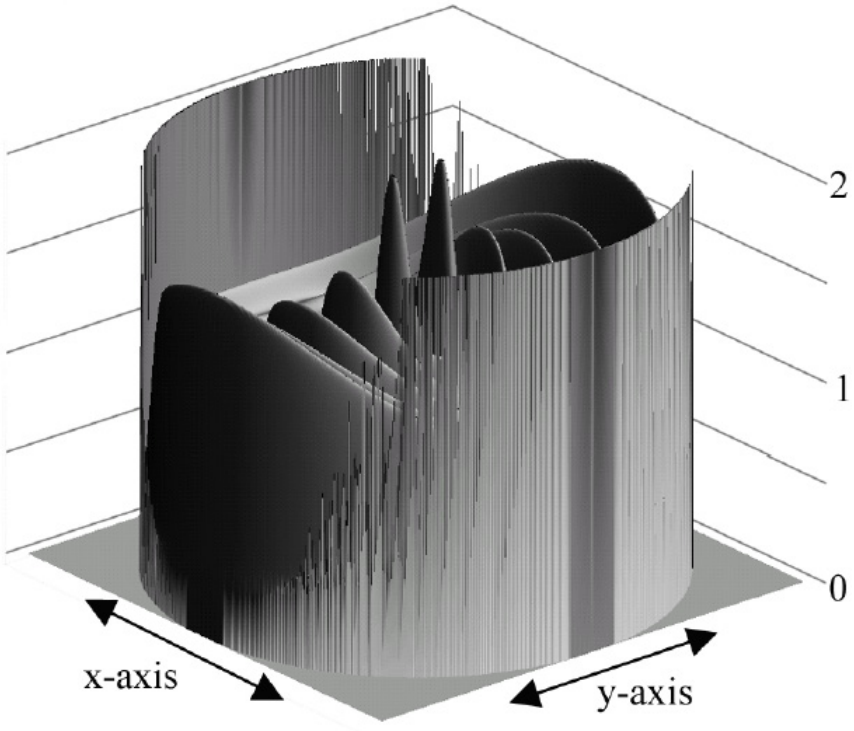


Fig. 4. Calculated modulus square of the $x$-component of the electric field ($|E_x/E_o|^2$) versus $x$ and $y$ in the aperture plane using single integral HVDT, $\sqrt{(x/a)^2+(y/a)^2} < 1$ and for $a/\lambda = 5$.

### *6.2. Beam distributions beyond the aperture plane*

#### 6.2.1. On-axis calculations

The analytical expressions obtained for the fields for on-axis points, $(x = y = 0)$, in Eqs. (78), (81), (84) and (85) provide an understanding of the behavior of the beam away from the aperture plane. In Fig. 10 the on-axis values of $S_z/S_o$ calculated using HVDT (Eqs. (78) and (81)) and KVDT (Eqs. (84) and (85)) are plotted along with the on-axis value of $|E_x/E_o|^2$ (from Eq. (78)) for $a/\lambda = 0.5$, 1, 2.5 and 5. As discussed before, for $a/\lambda > 1$ the on-axis intensity values go through a number of minima and maxima, with the total number of minima or maxima roughly equal to the value of $a/\lambda$ and the positions of the maxima or minima given by $z_1 \approx 1/(2m\pi)$ where the maxima occur for odd integer values of $m$ and the minima occur for even integer values of $m$. The last maximum (farthest from the aperture) occurs at $z_1 \approx 1/(2\pi)$, and for $z_1 \geq 1/(2\pi)$ the intensity drops off as $1/z_1^2$, corresponding to the spreading of a spherical wave.

For small $z_1$, i.e., in and near the aperture plane, the HVDT and KVDT results are different from each other and from $|E_x/E_o|^2$ for all the cases of $a/\lambda$, as shown in Fig. 10. However, the HVDT and KVDT results and $|E_x/E_o|^2$ come close to each other, even for $a/\lambda = 0.5$, for $z_1 > 0.2$. This implies that even for $a/\lambda \approx 0.5$, KVDT can be used to predict beam shapes at planes sufficiently far away from the aperture.

#6195 - $15.00 US Received 5 January 2005; revised 18 February 2005; accepted 18 February 2005
(C) 2005 OSA

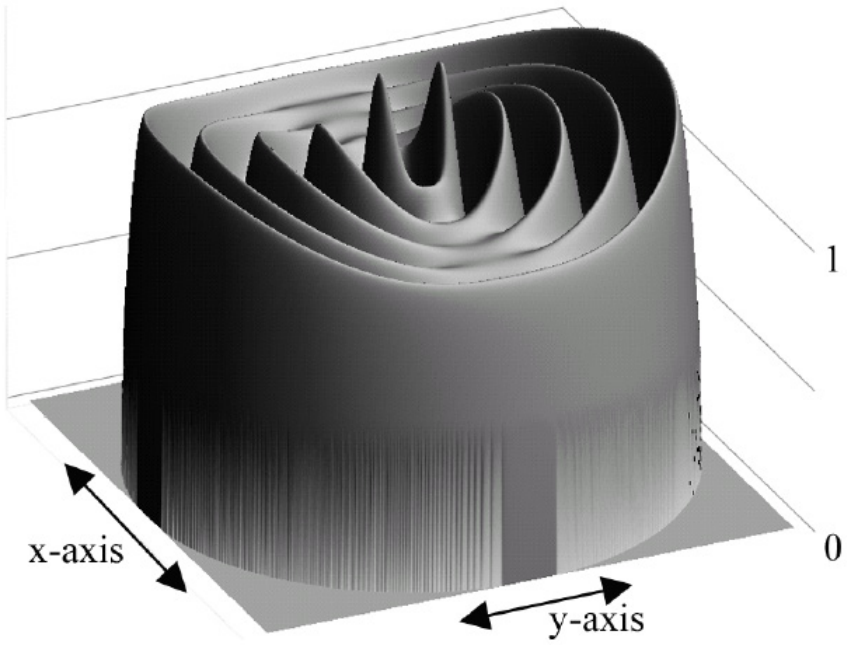


Fig. 5. Calculated $z$-component of the Poynting vector ($S_z/S_o$) versus $x$ and $y$ in the aperture plane using single integral HVDT, $\sqrt{(x/a)^2+(y/a)^2} < 1$ and for $a/\lambda = 5$.

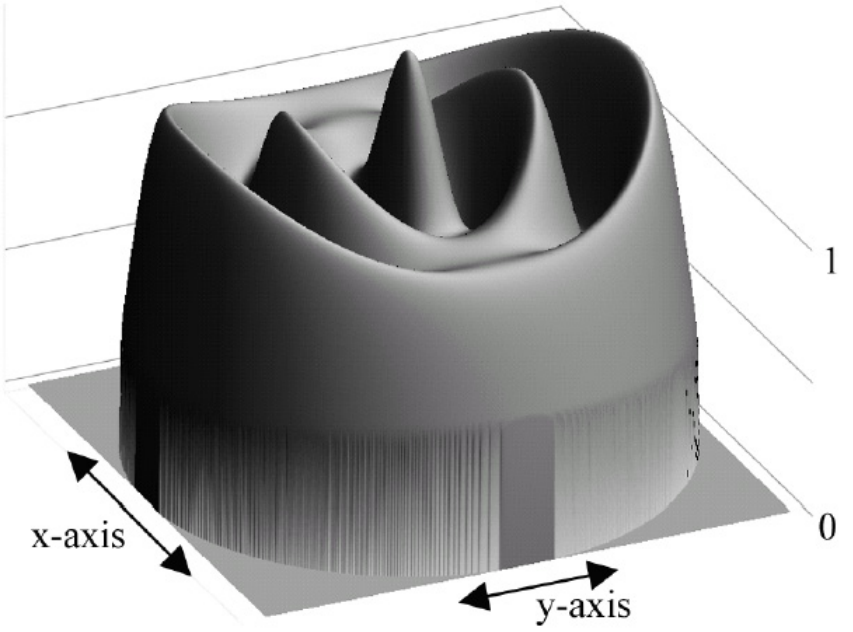


Fig. 6. Calculated $z$-component of the Poynting vector ($S_z/S_o$) versus $x$ and $y$ in the aperture plane using single integral HVDT, $\sqrt{(x/a)^2+(y/a)^2} < 1$ and for $a/\lambda = 2.5$.

#6195 - $15.00 US Received 5 January 2005; revised 18 February 2005; accepted 18 February 2005
(C) 2005 OSA

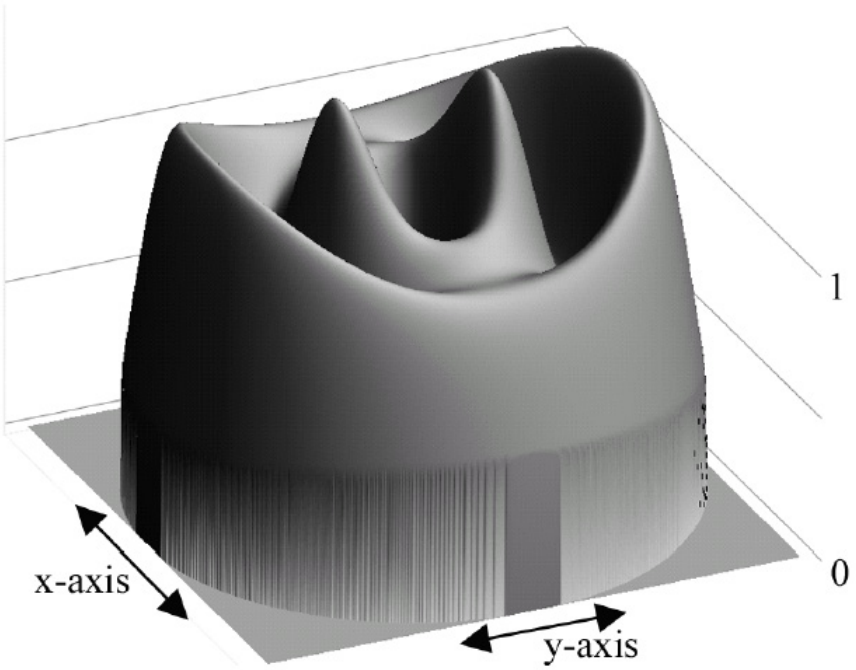


Fig. 7. Calculated $z$-component of the Poynting vector ($S_z/S_o$) versus $x$ and $y$ in the aperture plane using single integral HVDT, $\sqrt{(x/a)^2+(y/a)^2} < 1$ and for $a/\lambda = 2$.

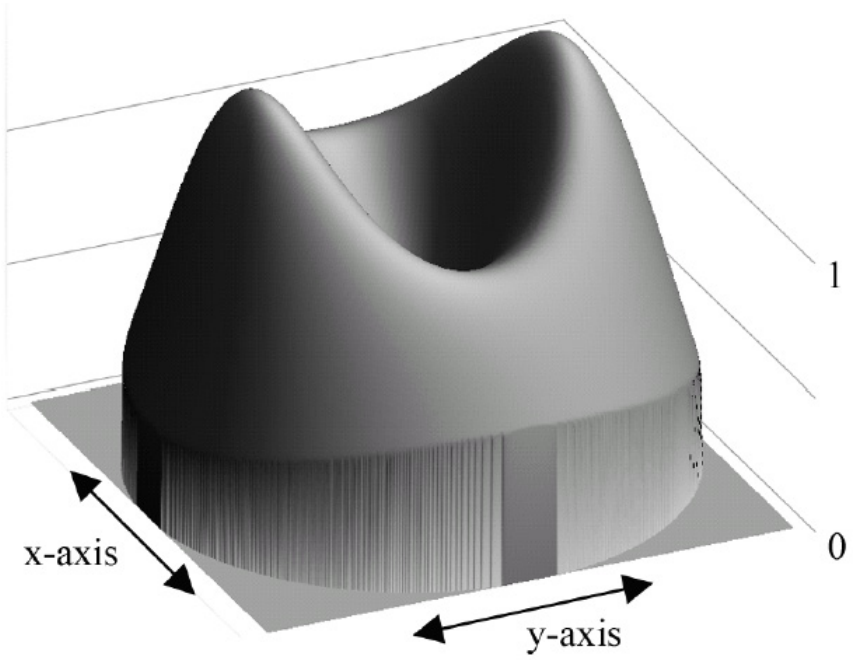


Fig. 8. Calculated $z$-component of the Poynting vector ($S_z/S_o$) versus $x$ and $y$ in the aperture plane using single integral HVDT, $\sqrt{(x/a)^2+(y/a)^2} < 1$ and for $a/\lambda = 1$.

#6195 - $15.00 US Received 5 January 2005; revised 18 February 2005; accepted 18 February 2005
(C) 2005 OSA

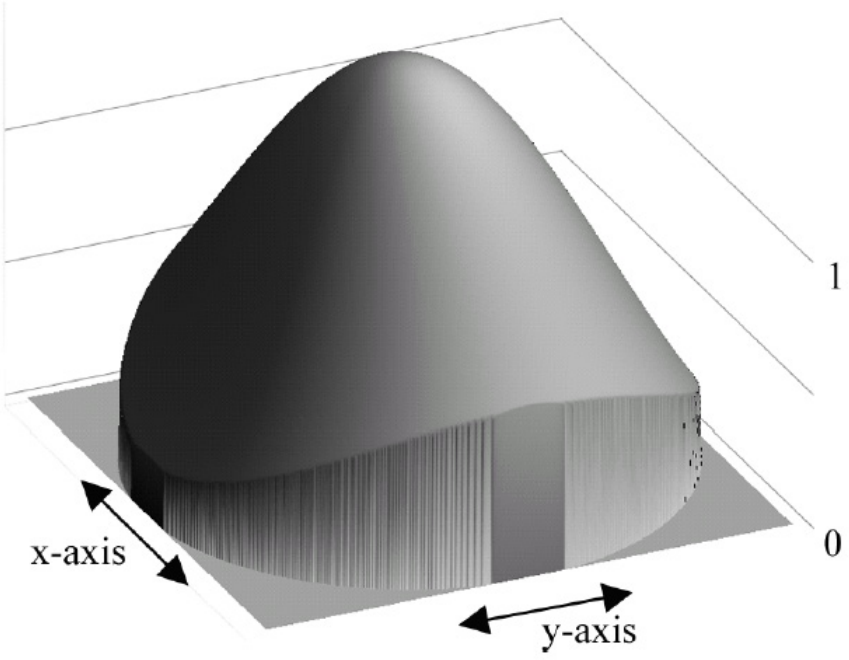


Fig. 9. Calculated $z$-component of the Poynting vector ($S_z/S_o$) versus $x$ and $y$ in the aperture plane using single integral HVDT, $\sqrt{(x/a)^2+(y/a)^2} < 1$ and for $a/\lambda = 0.5$.

6.2.2. Diffracted beam shapes

To determine if the radial asymmetry observed for $a/\lambda = 0.5$ in Fig. 9 persists as the beam propagates away from the aperture, the dependence of $S_z/S_o$ on the radial coordinate $r_1$ is plotted along the $x$ and $y$ axes in Figs. 11(a)–(c) for $a/\lambda = 0.5$ and in Figs. 11(d)–(f) for $a/\lambda = 5$ for three different values of $z_1$ ($10^{-4}$, 0.1 and 1). Figure 11(a)–(c) shows that for $a/\lambda = 0.5$, at the aperture plane ($z_1 = 10^{-4}$) the beam is elliptically shaped with the major axis in the $x$-direction. Results of calculation using the FDTD method (for $a/\lambda = 0.308$, at $z_1 = 0.052$) are shown in Ref. [18]. The plot of transmitted intensity "corresponding to $E_x$" in Fig. 10 of [18] also shows the radial asymmetry and the elongation of the beam along the $x$-axis. As the beam propagates, the ellipticity decreases and beyond $z_1 > 0.1$ the beam becomes elongated along the $y$-axis. The plots in Figs. 11(d)–(f) show that for larger $a/\lambda$ values, although the beam is strongly asymmetric near the aperture plane, as it propagates away from the aperture plane it becomes radially symmetric more quickly than for the smaller $a/\lambda$ case. Figures 12 and 13 show the detailed two-dimensional distribution of $S_z/S_o$ at the positions of an axial maximum ($z_1 = 1/(6\pi)$) and an axial minimum ($z_1 = 1/(4\pi)$), for $a/\lambda = 5$.

### *6.3. The longitudinal component of the electric field: $E_z$*

Along with the transverse field components, the Hertz vector theory allows the calculation of the longitudinal fields $E_z$ and $H_z$ as well. Since the incident unperturbed light beam is assumed to be a plane wave, it has no longitudinal field components. According to Eqs. 6c and 8 in Ref. [12], $E_z$ vanishes within the aperture at the aperture plane. Evaluation of the integral in Eq. (15) at various $x_1$, $y_1$ points within the aperture shows that the integral is independent of $z_1$ as $z_1$ approaches 0, so that $E_z$ is proportional to $z_1$. This verifies that (consistent with the

#6195 - $15.00 US Received 5 January 2005; revised 18 February 2005; accepted 18 February 2005
(C) 2005 OSA

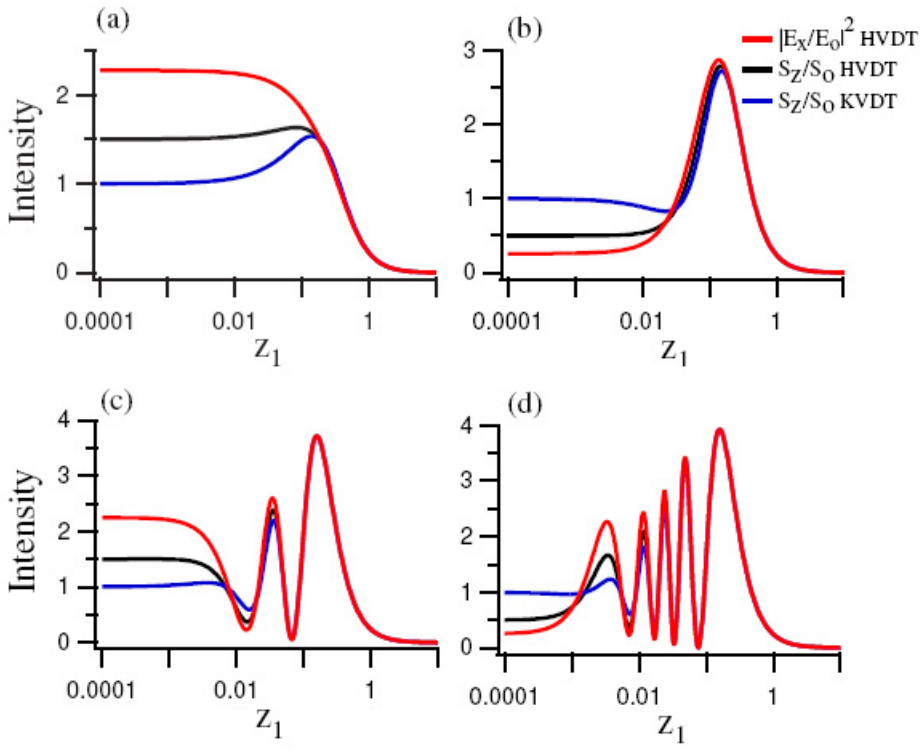


Fig. 10. Calculated on-axis values for the modulus square of the $x$-component of the electric field (red line) using HVDT, the $z$-component of the Poynting vector (black line) using HVDT, and the $z$-component of the Poynting vector (blue line) using KVDT for: (a) $a/\lambda = 0.5$, (b) $a/\lambda = 1$, (c) $a/\lambda = 2.5$ and (d) $a/\lambda = 5$.

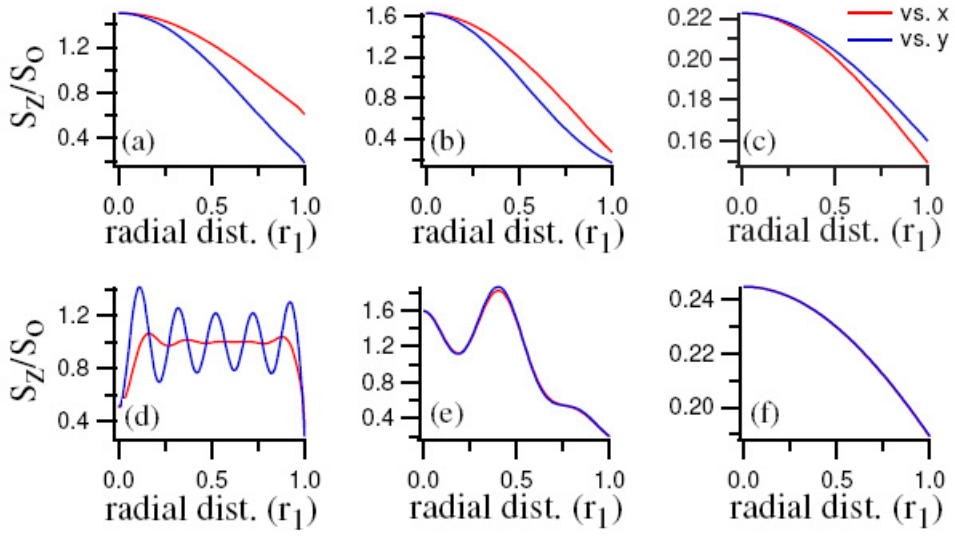


Fig. 11. Calculated $S_z/S_o$ for $a/\lambda = 0.5$ with (a) $z_1 = 10^{-4}$, (b) $z_1 = 0.1$, (c) $z_1 = 1$, and for $a/\lambda = 5$ with (d) $z_1 = 10^{-4}$, (e) $z_1 = 0.1$, and (f) $z_1 = 1$, using the single integral HVDT. The distance $r_1$ is either $x$ or $y$ normalized to the aperture radius, $a$.

#6195 - $15.00 US
Received 5 January 2005; revised 18 February 2005; accepted 18 February 2005
(C) 2005 OSA

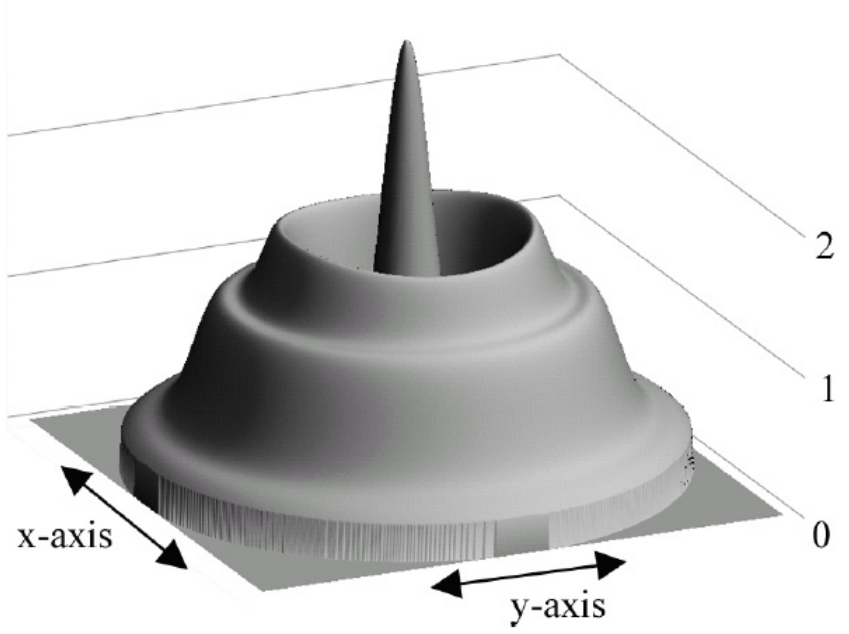


Fig. 12. Calculated $z$-component of the Poynting vector ($S_z/S_o$) versus $x$ and $y$ for $z_1 = 1/6\pi$ using the single integral HVDT, $\sqrt{(x/a)^2+(y/a)^2} < 1$ and $a/\lambda = 5$.

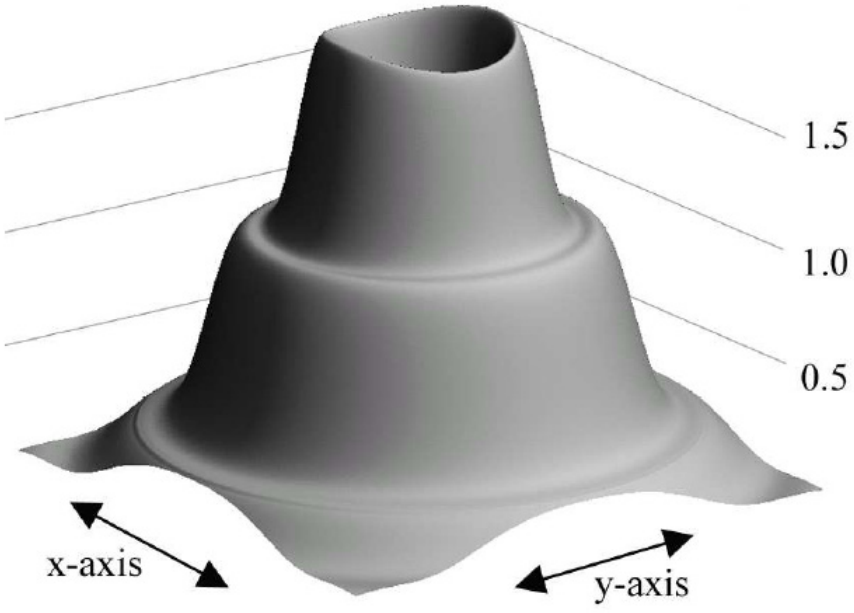


Fig. 13. Calculated $z$-component of the Poynting vector ($S_z/S_o$) versus $x$ and $y$ for $z_1 = 1/4\pi$ using the single integral HVDT for $a/\lambda = 5$.

#6195 - $15.00 US Received 5 January 2005; revised 18 February 2005; accepted 18 February 2005
(C) 2005 OSA

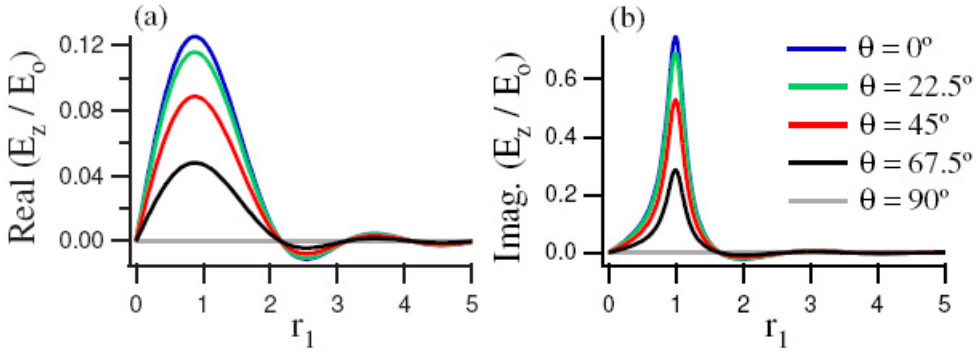


Fig. 14. Calculated real, (a), and imaginary, (b), components of $E_z/E_o$ for $\theta = 0^\circ$ ($x$-axis), 22.5°, 45°, 67.5° and 90° ($y$-axis), for $a/\lambda = 0.5$ and $z_1 = 0.05$.

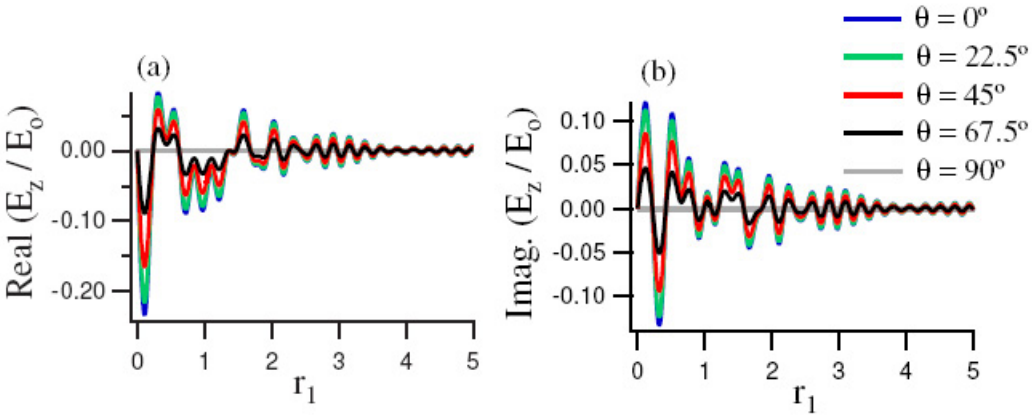


Fig. 15. Calculated real, (a), and imaginary, (b), components of $E_z/E_o$ for $\theta = 0^\circ$ ($x$-axis), 22.5°, 45°, 67.5° and 90° ($y$-axis), for $a/\lambda = 5$ and $z_1 = 0.05$.

requirement of Maxwell's equations) $E_z$ vanishes in the aperture plane, i.e., when $z_1 \to 0$. Here we present the results of some calculations showing distribution of $E_z/E_o$ at various distances near the aperture. Figures 14 and 15 show the dependence of $E_z/E_o$ on the radial coordinate $r_1$ for various values of the angular coordinate $\theta$, for $a/\lambda = 0.5$ and 5 respectively, at a distance of $z_1 = 0.05$. It is seen that the maximum value of both the real and the imaginary parts of $E_z/E_o$ (for both values of $a/\lambda$) are obtained for $\theta_1 = 0$, i.e., along the $x$-axis. Figures 16 and 17 show the dependence of $E_z/E_o$ on $x_1$ (for $y_1 = 0$) at various distances from the aperture ($z_1 = 0.05$, 0.1, 0.5, and 1) for $a/\lambda = 0.5$ and 5, respectively. It is seen that even for $a/\lambda = 5$, the $E_z$ can be a substantial fraction (20 percent) of the incident field amplitude at certain positions in front of the aperture.

### *6.4. Power transmission function calculations*

Evaluating $T$ using Eq. (90) for different $z_1$ values shows that for fields calculated using HVDT, $T$ is independent of $z_1$. In contrast, if the fields calculated using KVDT are used to calculate $P_z$, the value of $T$ depends upon $z_1$, thus showing that the Kirchhoff assumption is in violation of the conservation of energy principle as well as of the Maxwell's equations.

#6195 - $15.00 US
Received 5 January 2005; revised 18 February 2005; accepted 18 February 2005
(C) 2005 OSA

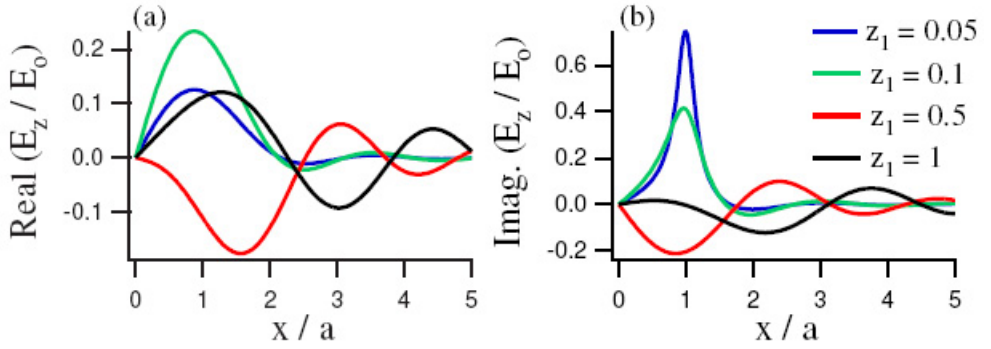


Fig. 16. Calculated real, (a), and imaginary, (b), components of $E_z/E_o$ along the $x$-axis for $z_1 = 0.05$, 0.1, 0.5 and 1, for $a/\lambda = 0.5$.

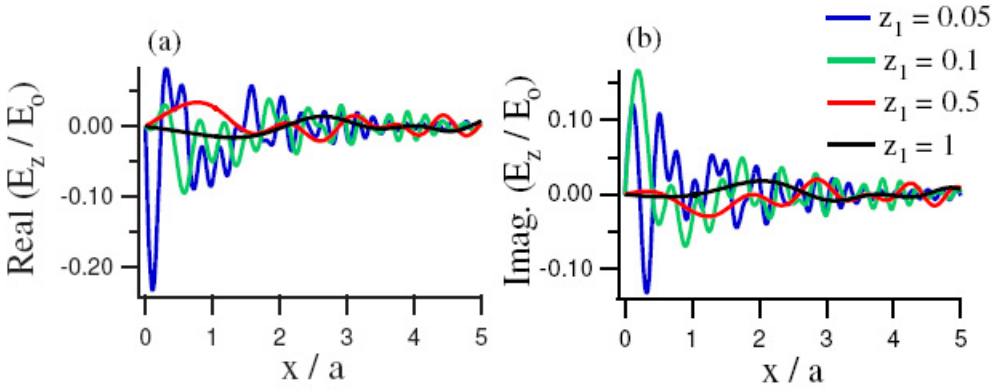


Fig. 17. Calculated real, (a), and imaginary, (b), components of $E_z/E_o$ along the $x$-axis for $z_1 = 0.05$, 0.1, 0.5 and 1, for $a/\lambda = 5$.

Figure 18 shows a plot of $P_z/P_o$ calculated using Eq. (90) as a function of $a/\lambda$. For $a/\lambda < 0.5$ the power transmitted by the aperture decreases monotonically with decreasing $a/\lambda$. For $a/\lambda > 0.5$, the transmitted power oscillates weakly and in general increases with increasing $a/\lambda$ and asymptotically approaches unity. However, as shown in the insert of Fig. 18, even for $a/\lambda = 10$, the value of $T$ is less than 1 (in fact is equal to 99.2%).

## 7. Conclusions

Expressions for the electric and magnetic fields of a plane wave incident on a circular aperture have been presented here in the form of double integrals as well as single integrals using the Hertz vector diffraction theory. The expressions for the fields obtained using the Kirchhoff boundary conditions are also presented. Detailed numerical calculations for the field and intensity distributions at the aperture plane and away from the aperture plane are presented. The range of validity of the theory presented here is for an aperture to wavelength ratio of $\approx 0.5$ and higher. It is shown that at and very near the aperture plane, the Kirchhoff boundary conditions are *never* valid, even for arbitrarily large values of the aperture to wavelength ratio. However, at a certain distance from the aperture, the results obtained from the Kirchhoff approximation and that obtained using the more detailed Hertz vector formalism, which intrinsically obeys

#6195 - $15.00 US Received 5 January 2005; revised 18 February 2005; accepted 18 February 2005
(C) 2005 OSA

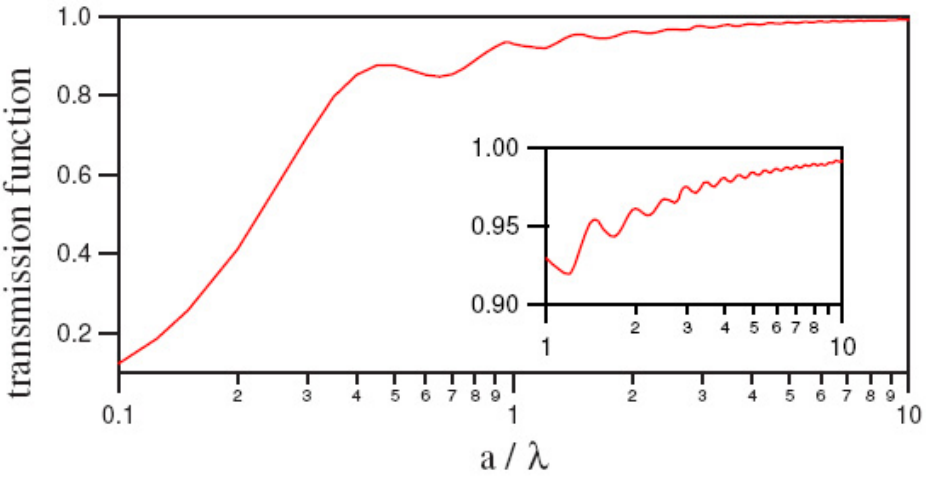


Fig. 18. Calculated transmission function as a function of the aperture radius to wavelength of light ratio, calculated using HVDT.

Maxwell's equations, are about identical, even for aperture to wavelength ratios as small as 0.5. Radial asymmetry of the electric field distribution for small circular apertures have been experimentally demonstrated before. Here we have presented, for the first time to our knowledge, calculations of the detailed two-dimensional field and intensity distributions, along with the calculation of the longitudinal component ($E_z$) of the electric field using the Hertz vector diffraction theory.

Schoch [16] has shown that the double integral of $\Pi_x$ in Eq. (6) over a surface can be transformed into a line integral along the aperture edge for an aperture of arbitrary shape. The method described here for a circular aperture can therefore be extended to elliptical or rectangular apertures.

**Acknowledgment**

The authors thank Prof. Wolfgang Freude of Universität Karlsruhe for pointing out to them the limitations of the Kirchhoff boundary conditions at the Annual Meeting of the Optical Society of America, Rochester, New York, October 2004.

#6195 - $15.00 US Received 5 January 2005; revised 18 February 2005; accepted 18 February 2005
(C) 2005 OSA